

Geophysical Research Letters[®]



RESEARCH LETTER

10.1029/2023GL104714

MMS Observation of Two-Step Electron Acceleration at Earth's Bow Shock

M. Lindberg¹ , A. Vaivads^{1,2} , S. Raptis^{1,3} , and T. Karlsson¹ 

¹Division of Space and Plasma Physics, KTH Royal Institute of Technology, Stockholm, Sweden, ²Ventspils University of Applied Sciences, Ventspils, Latvia, ³The Johns Hopkins University Applied Physics Laboratory, Laurel, MD, USA

Key Points:

- Using Magnetospheric Multiscale data we observe bi-directional energetic electrons at Earth's collisionless bow shock
- The observations are inconsistent with common electron acceleration mechanisms at shocks
- We propose a two-step acceleration process where a field-aligned electron beam is further accelerated by a shrinking magnetic bottle

Correspondence to:

M. Lindberg,
mlif6@kth.se

Citation:

Lindberg, M., Vaivads, A., Raptis, S., & Karlsson, T. (2023). MMS observation of two-step electron acceleration at Earth's bow shock. *Geophysical Research Letters*, *50*, e2023GL104714. <https://doi.org/10.1029/2023GL104714>

Received 31 MAY 2023

Accepted 7 AUG 2023

Author Contributions:

Conceptualization: M. Lindberg, A. Vaivads

Data curation: M. Lindberg, S. Raptis
Formal analysis: M. Lindberg

Investigation: M. Lindberg, A. Vaivads

Methodology: M. Lindberg, A. Vaivads

Project Administration: A. Vaivads

Software: M. Lindberg, S. Raptis

Supervision: A. Vaivads, T. Karlsson

Validation: T. Karlsson

Visualization: M. Lindberg

Writing – original draft: M. Lindberg

Writing – review & editing: M. Lindberg, A. Vaivads, S. Raptis

Lindberg, A. Vaivads, S. Raptis

Abstract We use the Magnetospheric Multiscale mission to observe a bi-directional electron acceleration event in the electron foreshock upstream of Earth's quasi-perpendicular collisionless bow shock. The acceleration region is associated with a decrease in wave activity, inconsistent with common electron acceleration mechanisms such as Diffusive Shock Acceleration and Stochastic Shock Drift Acceleration. We propose a two-step acceleration process where an electron field-aligned beam acts as a seed population further accelerated by a shrinking magnetic bottle process, with the shock acting as the magnetic mirror(s).

Plain Language Summary Collisionless shock waves are believed to be an important source of accelerating particles up to cosmic ray energies throughout our universe. In this letter, we use spacecraft data from the Magnetospheric Multiscale mission to study an energetic electron event observed at Earth's bow shock. The event displays inconsistencies with common electron acceleration mechanisms previously studied at collisionless shocks. We propose a two-step acceleration mechanism, combining two known mechanisms for charged particle acceleration, and provide observational evidence supporting our theory. We conclude that plasma wave-particle interactions at the shock play a crucial role in the energization of these electrons.

1. Introduction

Collisionless shock waves are important sources of particle acceleration throughout the universe. There are still many open questions about the acceleration mechanism for both ions and electrons. Ion acceleration has been studied with great success the recent years and heliospheric observations suggest more efficient acceleration than electrons (Amano et al., 2020; Johlander et al., 2021; Stasiewicz & Kłos, 2022). Electron acceleration remains to a greater extent unsolved. The diffusive shock acceleration (DSA) process successfully explains how electrons can be Fermi-accelerated up to relativistic cosmic ray energies (Balogh & Treumann, 2013b). However, this process only occurs if the electrons already have sufficiently high energy. Therefore, electrons have to be pre-accelerated via other mechanisms up to mildly relativistic energies 0.1–1 MeV before they can be further accelerated through the DSA process (Amano & Hoshino, 2022). This is known as the injection problem, and much effort has been put into solving it over the last decades.

Because of the complex dynamics of collisionless shocks, a lot of effort has been put into simulations (Bohdan et al., 2020; Guo & Giacalone, 2015; Hoshino & Shimada, 2002; Lembège & Savoini, 2002; Matsumoto et al., 2017; Trotta & Burgess, 2019). Particle-in-cell (PIC) and test particle simulations are powerful tools for studying electron acceleration at astrophysical shocks. Their results can be verified from real data using either remote sensing techniques or in situ measurements. Observations of synchrotron radiation in young supernova remnant shocks suggest electrons are being efficiently accelerated up to ultra-relativistic energies (Bamba et al., 2005; Koyama et al., 1995). On the other hand, in situ measurements at heliospheric shocks (e.g., Earth's bow shock and solar coronal shocks) indicate that relativistic electrons with energies above 1 MeV are rare within the heliosphere (Dresing et al., 2016, 2022; Turner et al., 2016; Wilson et al., 2016), suggesting different efficiency of electron acceleration at different types of shocks. The large difference in spatial and temporal scales, comparing heliospheric and astrophysical shocks, plays an important role in which physical acceleration processes are likely to be efficient.

The stochastic shock drift acceleration (SSDA) mechanism is currently the most promising candidate for a solution to the electron injection problem (Amano & Hoshino, 2022). SSDA adds to the general SDA theory by introducing a stochastic process where the accelerated electrons are pitch-angle scattered by whistler waves in the shock transition layer, allowing electrons to undergo the SDA process longer and hence gain more energy.

© 2023. The Authors.

This is an open access article under the terms of the [Creative Commons Attribution License](https://creativecommons.org/licenses/by/4.0/), which permits use, distribution and reproduction in any medium, provided the original work is properly cited.

Theoretical studies (Katou & Amano, 2019) show that this method can produce a power law spectrum for suprathermal electrons, supported by observational evidence (Amano et al., 2020).

This paper presents a case of energetic electron acceleration that cannot be explained by the SSDA mechanism and requires an alternative electron acceleration process. The accelerated electrons are observed upstream of a quasi-perpendicular shock where the wave activity is minimal and therefore inconsistent with the SSDA model. We show evidence of a two-step acceleration process where a field-aligned electron beam in the electron foreshock (Fitzenreiter, 1995; Pulupa et al., 2011) acts as a seed population further accelerated by a shrinking magnetic bottle process.

2. Observation

We analyze in detail the shock crossing as observed by the magnetospheric multiscale (MMS) spacecraft on the 7th of December 2018 around 11:51:20 UTC. MMS crosses the Earth's bow shock from the downstream magnetosheath to the upstream solar wind. This crossing is selected from over 1000 MMS shock crossings in the database created by Lalti, Khotyaintsev, Dimmock, et al. (2022). It displays one of the highest fluxes of energetic electrons, measured in the energy range 10–20 keV.

Figure 1 depicts the crossing as observed by MMS1. We identify the shock at 11:51:20 UTC from the steep rise in the magnetic field and density observed in Figures 1a and 1c. The high-energy electrons are observed upstream of the shock, seen as a large increase in the electron differential energy flux in Figures 1e and 1f between 11:51:35–11:51:45 UTC. The region is marked by yellow and will henceforth be denoted as the electron acceleration region (EAR). The flux enhancement is slightly detached from the shock transition layer and is also registered in the lowest energy channel of the high-energy electron flux plotted in Figure 1e. The flux enhancement appears just at the edge of the shock foot region, recognized by the appearance of high energetic ions and whistler wave activity in the magnetic field around 11:51:30 UTC (see Figures 1a and 1d). Further upstream, around 11:52:00 UTC, MMS observes an increase in wave activity associated with a rotation in the upstream magnetic field, and an increase of energetic ions is observed (see Figure 1d). We interpret this as an encounter with the ion foreshock that appears due to the change in the local shock angle. The local shock angle, shown in Figure 1j, is calculated using a 1-s sliding mean of the locally measured magnetic field plotted in Figure 1a and a shock normal obtained by averaging over the four bow shock models in Slavin and Holzer (1981), Peredo et al. (1995), Fairfield (1971), and Formisano (1979). The shock angle, θ_{Bn} , changes from 70 to 80° down to 40–50° and then back to around 80° between 11:51:45 and 11:52:20 UTC. This rotation modifies the region upstream of the shock from quasi-perpendicular to quasi-parallel and back to quasi-perpendicular (Balogh & Treumann, 2013a). During the period of quasi-parallel configuration, we observe energetic ions above 10 keV, consistent with earlier observations at quasi-parallel shocks (Balogh & Treumann, 2013c; Burgess et al., 2005; Johlander et al., 2021; Stasiewicz & Klos, 2022).

Figure 2 shows the spacecraft location along with the bow shock model and upstream magnetic field direction obtained by OMNI measurements. The spacecraft position, upstream magnetic field direction, and the high-energy electron fluxes observed throughout the whole time interval (see Figure 1f) suggest that the spacecraft is crossing the shock into the electron foreshock region.

This region contains energetic electrons accelerated into field-aligned beams (FAB) originating from the magnetic field/shock tangential point. Although the exact mechanism of the FAB is not entirely understood (Meziane, 2005; Vandas, 2001), it is suggested that the FAB is created by SDA (Leroy & Mangeney, 1984; Wu, 1984) of particles at the nearly perpendicular shock occurring at the magnetic field/shock tangential point. However, numerical simulations report that electron energy gain at supercritical shocks is much higher than that predicted by adiabatic reflection theory (Burgess, 2006; Krauss-Varban et al., 1989; Trotta & Burgess, 2019).

Figures 1g–1i shows pitch-angle distributions averaged over specific energy intervals. The distributions show a bi-directional electron population at the EAR, visible from 200 eV up to 20 keV. It displays relatively constant energy flux for pitch angles above and below 120 and 60° while being roughly one order of magnitude less for pitch angles between 70 and 110°. Note the asymmetric distributions to the left and right of the EAR, where a flux enhancement is seen anti-parallel to the B-field. We interpret this as the characteristic signature of the FAB (Pulupa et al., 2011).

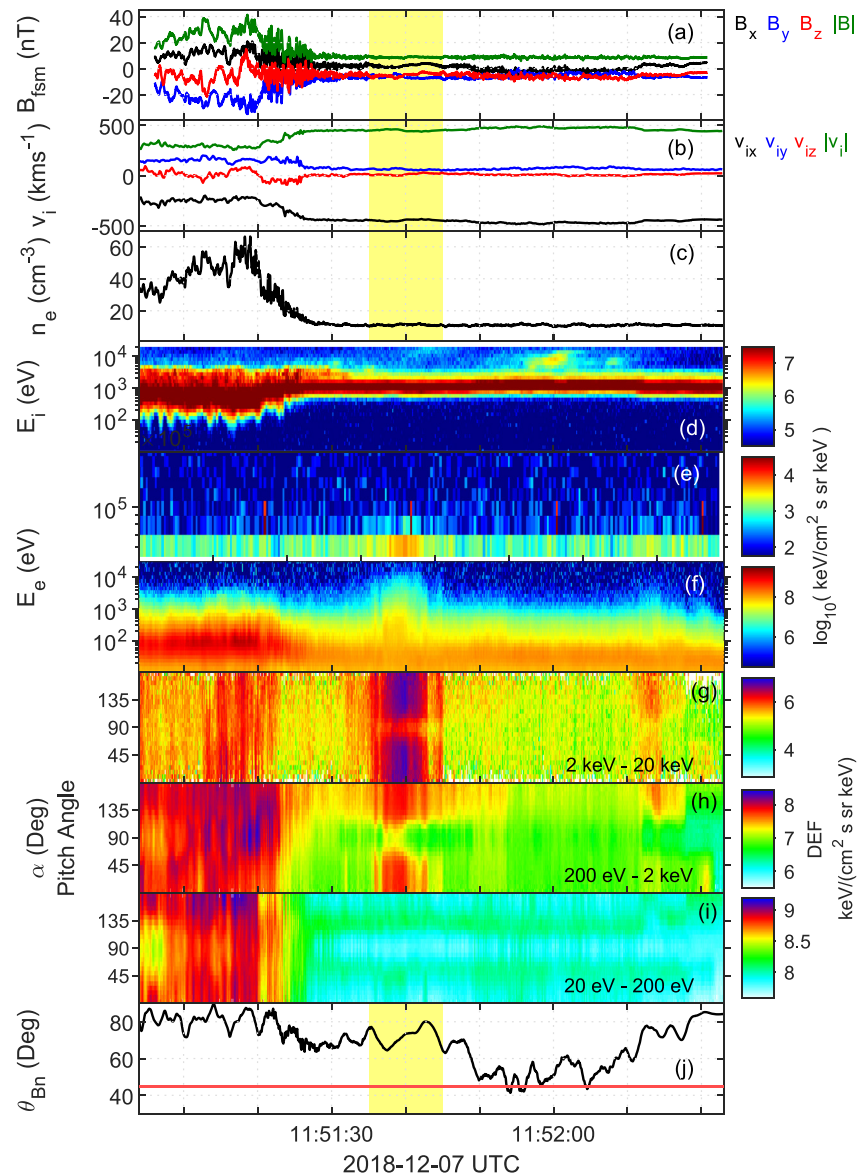


Figure 1. MMS measurements of the shock crossing. The panels show, (a) magnetic field, (b) ion velocity, (c) electron density, (d) ion spectrogram, (e) high-energy electron spectrogram, (f) electron spectrogram, (g–i) energy averaged pitch-angle distributions, (j) shock angle, θ_{Bn} . The yellow background indicates the electron acceleration region (EAR). All panels show data from the MMS1 spacecraft except panels (g–i) where an average over MMS1–3 is used.

3. Theory

The large increase in electron differential flux at the EAR combined with bi-directional pitch-angle distribution strongly suggests trapped electrons. Bi-directional particle distributions have been observed in ISEE data (Bame et al., 1981) and used as evidence for magnetic bottle configurations (Palmer et al., 1978). Therefore, we suggest electrons are accelerated in a two-step process where the electron FAB acts as a seed population injected into a shrinking magnetic bottle. The concept is illustrated in Figure 3a.

Consider a deformation (Johlander et al., 2016, 2018; Kajdič et al., 2019; Madanian et al., 2021) of the shock surface occurring near the field line/shock tangential point where the FAB originates. The electrons are accelerated via conventional SDA (Vandas, 2001; Wu, 1984) along the field lines. Meanwhile, the field lines are convected across the shock, causing the electrons to be trapped on field lines intersecting the shock at two locations (see Figure 3a). This type of magnetic loop structure has been studied in Giacalone (2005) and Decker (1993) where

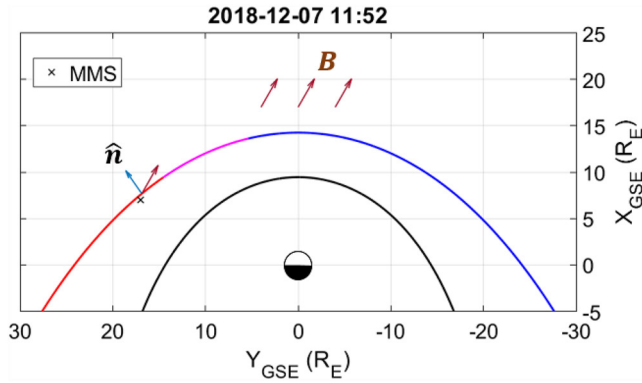


Figure 2. MMS location, magnetopause (black curve), and bow shock model at 2018-12-07 11:52 UTC. The small black cross indicates the spacecraft's location and the brown arrows show the upstream magnetic field direction in the GSE XY-plane. The models are obtained using ± 1 measurements from the Slavin and Holzer (1981) model. The colors represent the different regions where $\theta_{Bn} > 50^\circ$ (red), $40^\circ < \theta_{Bn} < 50^\circ$ (magenta) and $\theta_{Bn} < 40^\circ$ (blue).

similar enhancement of particle flux and bi-directional pitch-angle distribution was observed. As the field lines continue to convect across the shock, the magnetic loop starts to shrink and the two field-line-shock intersections (shrinking mirror points in Figure 3a) start to approach each other. Such configuration can accelerate the FAB-generated electrons further through multiple reflections between the shock, acting as two magnetic mirrors. From the conservation of the second adiabatic invariant, the increase in energy for a trapped electron in a shrinking magnetic bottle is given by

$$\frac{w_f}{w_i} = \frac{B_{mf}}{B_{mi}} \quad (1)$$

where w_f and w_i are the final and initial electron energies and B_{mf} and B_{mi} are the final and initial mirror point magnetic field strength (Gurnett & Bhattacharjee, 2005). Assuming a simple magnetic bottle-like geometry illustrated in Figure 3b, the maximum increase in electron energy can be estimated using Equation 1. The maximum gain in energy an electron can obtain occurs when the final mirror point is the maximum field strength at the shock and the initial point is the upstream field strength. Taking the final mirror point field strength, B_{mf} , as the average of the 10 maximum magnetic field measurements for each of the four MMS-spacecraft over the shock interval (11:51:10–11:51:30 UTC) and B_{mi} as the average over the EAR (11:51:35–11:51:45 UTC) yields

$$\frac{w_f}{w_i} = \frac{B_{\max}}{B_{\min}} = \frac{40 \pm 1.6}{8.6 \pm 0.4} = 4.6 \pm 0.3. \quad (2)$$

Generally, the energy gain is expected to be less than the value obtained in Equation 2. We obtain the change in electron energy, w_f/w_i , by studying the distribution functions. Figures 4a and 4b shows measured distribution functions from the EAR (green) and background electron foreshock/FAB (red). According to the Sturm-Liouville theorem (Paschmann & Daly, 2000), the distribution function is constant along the particle orbit. Hence, the shift in energies of the two curves indicates the increase in energy of the reflected FAB electrons through the shrinking magnetic bottle. Figure 4c displays the energy gain as a function of energy, obtained by comparing the two distribution functions in panel (b) for constant f -values. It can be seen that the increase in electron energy is strictly less than the maximum limit obtained from the simple adiabatic model stated in Equation 2. Note that the energy gain efficiency is smaller for low energy than high energy electrons, see Figure 4c. This can be explained by low-energy electrons having too low speed to undergo any reflection.

When considering the simplified shrinking magnetic bottle theory used to derive Equation 1 and illustrated in Figure 3b, the theory predicts the existence of a loss cone where electrons within the loss cone escape the bottle configuration. The loss cone is given by $\sin^2 \alpha = B_{\min}/B_{\max}$. Using the same magnetic field strengths above gives a loss cone angle of $\alpha = 27 \pm 1^\circ$. The pitch-angle distributions at the EAR in Figures 1g and 1h, do not show a loss cone. Thus, a simplified magnetic bottle model cannot explain the observations.

We suggest that the shrinking magnetic bottle model can still explain observations if the particle reflection is not only due to the adiabatic magnetic mirroring but large amplitude wave pitch-angle scattering. This is illustrated in Figure 3c. The shock transition layer contains several different kinds of plasma waves that can pitch-angle scatter electrons (Amano et al., 2020; Vasko et al., 2018). The magnetic field data in Figure 1a displays wave magnetic field amplitudes over 10 nT where the background magnetic field is 13 nT. Such large amplitude waves can efficiently pitch-angle scatter electrons (Blandford & Eichler, 1987), enabling escaping electrons to be reflected back upstream into the bottle region. It is known that non-linear whistler waves upstream of quasi-perpendicular shocks can reflect electrons (Balikhin et al., 1989) and Amano et al. (2020) showed observational evidence for electron pitch-angle scattering by whistler waves at the Earth's bow shock. Following Amano et al. (2020), we calculate the pitch-angle scattering rate, D_{scat} , at the shock and compare it to a theoretical threshold obtained using quasi-linear theory (Katou & Amano, 2019). The result is depicted in Figure 4d showing a scattering rate higher than the threshold for electron energies between 50 eV up to 3 keV.

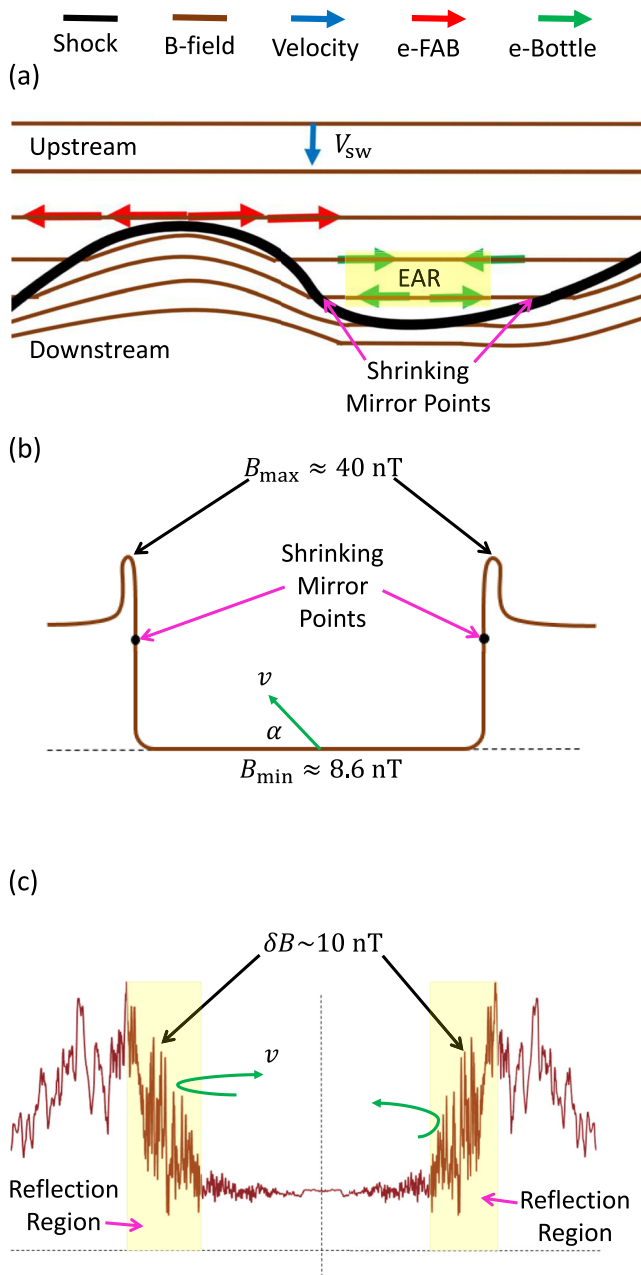


Figure 3. (a) Illustration of the two-step acceleration theory proposed in this study. A deformation on the shock surface (black) causes field lines to intersect the shock at two different locations. As the magnetic field lines (brown) are convected with the bulk flow (blue arrow) toward the shock, field-aligned accelerated electrons (red arrows) are trapped between the shrinking magnetic mirror points (green arrows). (b) Simplified adiabatic model of a shrinking magnetic bottle. (c) A more realistic model where pitch-angle scattering at the shock is considered on top of the adiabatic reflection.

The threshold indicates the pitch-angle scattering rate at which the electron diffusion length equals the length of the shock transition layer (Amano & Hoshino, 2022; Amano et al., 2020; Katou & Amano, 2019). Therefore, a scattering rate above this threshold indicates strong pitch-angle scattering and a loss cone is not expected. The time interval defined as the shock transition region producing Figure 4d, following Amano et al. (2020), was chosen between 11:51:[20–28] UTC.

Alternatively, the characteristic pitch-angle scattering time can be estimated from the wave amplitudes present at the shock (Crooker et al., 1999; Perri & Zimbardo, 2012)

$$\tau = \frac{2\pi}{D_{\alpha\alpha}} = \left(\frac{B_0}{\delta B}\right)^2 \frac{1}{f_{ce}}. \quad (3)$$

This expression gives the characteristic time for electron pitch angles to be scattered within 2π radians via cyclotron resonance. We estimate the $\delta B/B_0$ -term in Equation 3 as the normalized standard deviation (Crooker et al., 1999; Perri & Zimbardo, 2012) over the interval 11:51:21 to 11:51:26 UTC. For the 5 s time interval stated above we obtain $\delta B \approx 7.7$ nT, $B \approx 17.5$ nT and $f_{ce} \approx 500$ Hz. This gives a characteristic time of $\tau \approx 10$ ms which, for an electron with energy E , corresponds to efficient scattering distance along the background magnetic field

$$L = v_e \tau \approx 6\sqrt{E} \quad [\text{km}]. \quad (4)$$

where E is given in eV. This length has to be less than the distance traveled by electrons through the region where the waves are present. Using the 5 s time interval above, we estimate

$$L_{\text{sh}} = \frac{5 \text{ s} \cdot V_{\text{sh}}}{\cos\theta_{\text{Bn}}} \approx 1300 \text{ km} \quad (5)$$

where the shock velocity $V_{\text{sh}} = 27$ km/s and $\theta_{\text{Bn}} = 84^\circ$ are decided from multi-spacecraft methods (Paschmann & Daly, 2000). Comparing Equations 4 and 5, electrons with energies less than 40 keV will have a characteristic length $L < 1,200 \text{ km} < L_{\text{sh}}$ and can be expected to be completely pitch-angle scattered.

Due to the small separation of the MMS spacecraft, making reliable estimates of the geometry and size of the magnetic configuration is difficult using multi-spacecraft methods. However, the length of the magnetic field line between the two mirror points, L_b , can be estimated using Fermi-acceleration theory and the observational time of the bi-directional signature, $\Delta t \approx 5$ s. As seen from Figure 4, the effect of the bottle (bi-directional signature) is first observed around 100 eV. If we define the 100 eV electrons to (during Δt) only have time to perform two bounces and return to their starting position, we obtain

$$2L_b = \frac{2}{\pi} \int_0^{\pi/2} v_{\parallel}(\alpha) d\alpha \cdot \Delta t = \frac{2}{\pi} \cdot 5930 \cdot 5 \quad [\text{km}] \quad (6)$$

where α is the pitch angle and averaged over. Solving Equation 6 for the bottle length yields $L_b \approx 9,400$ km which corresponds to 130 upstream ion inertial lengths.

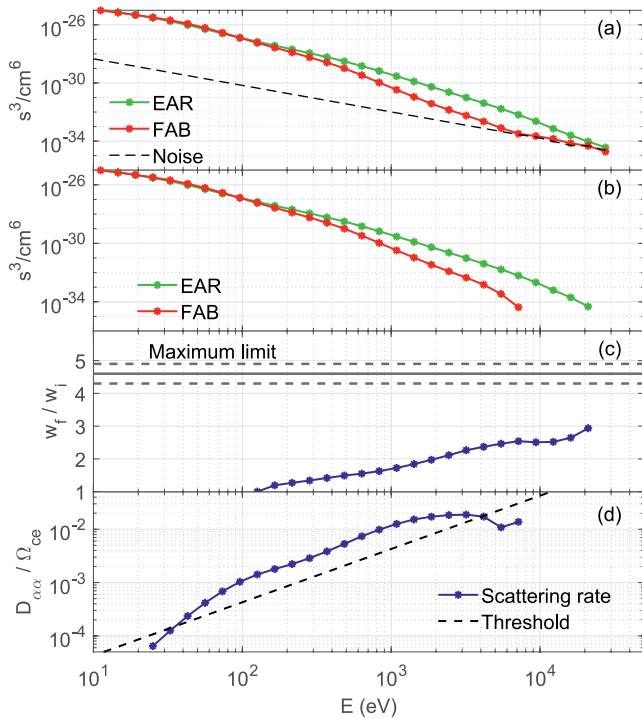


Figure 4. (a) Distribution functions of the EAR at 11:51:[38–41] (green) and field-aligned beams (FAB) at 11:51:[49–52] (red) together with estimated noise level (black). (b) Same distributions as in panel (a) but with noise level subtracted. (c) Increase in electron energy between the FAB and the EAR, calculated from the shift in distributions shown in panel (b). The solid (dashed) black line(s) indicate the maximum gain in energy (standard deviations) possible considering a magnetic bottle configuration illustrated in Figure 3(b). (d) The blue curve shows the pitch-angle diffusion (scattering) rate at the shock, while the black dashed line shows a theoretical threshold where the pitch-angle diffusion rate equals the width of the shock transition layer. The distributions are averaged over MMS1-3, solid angle, and 3-s time intervals (stated above). The noise level is determined by a linear fit of the five last data points on the red curve shown in panel (a).

at the turbulent region are much less than at the shock and the flux should then appear significantly weaker for pitch angles less than 90° . This feature is observed in Figure 1h around 11:51:50 and 11:52:12 and is interpreted as reflected electrons from the turbulent region.

Although the theory presented in this letter agrees with the data, more work needs to be done to verify it and evaluate its universality and ubiquity. The configuration of a magnetic loop intersecting a shock at two locations has been studied using simulations (Decker, 1993; Giacalone, 2005) and bi-directional electron populations have been reported by Palmer et al. (1978). Such configurations are more common at traveling interplanetary (IP) shocks and young supernova shocks than at the Earth's bow shock, and more in situ observations are needed to prove the geometry and size of the magnetic field configuration.

The illustration shown in Figure 3a portrays a deformed shock surface and offers one probable situation where the magnetic bottle configuration can occur. Alternatively, the same scenario can be obtained if the convecting solar wind magnetic field lines are curved. With the current data set, we cannot distinguish between the two scenarios. However, future missions with spacecraft simultaneously at large and small scales may distinguish both scenarios (Retinò et al., 2021). We estimate the size (field line length) of the configuration to be around 130 upstream ion inertial lengths. Previous studies by Kajdič et al. (2019) show shock corrugations at IP shocks up to 100 upstream ion inertial lengths. Therefore, if the bottle configuration mainly is caused by a shock deformation, it needs to be of a large-scale type. Also, recent work by Trotta et al. (2021) and Kajdič et al. (2021) indicates that upstream

4. Discussion

The evidence for strong pitch-angle scattering presented above suggests that no loss cone should be expected within the energy range considered. This is consistent with the pitch-angle distributions shown in Figures 1g and 1h. We conclude that the process needs to be completely stochastic where the adiabatic reflection caused by the mirror force is modified by a pitch-angle scattering process at the shock. Thus, causing an effective Fermi-type acceleration initiated by a magnetic field line loop intersecting the shock at two locations.

The pitch-angle scattering at the magnetic mirrors (shock) is essential for the two-step process. It allows the FAB-accelerated electrons to take part in the shrinking magnetic bottle longer before escaping and it determines the process's maximum energy gain. According to Equation 4, this energy should be slightly above 47 keV, that is, when the length obtained in Equation 4 exceeds the one in Equation 5. Figure 1e shows that the high electron differential energy flux signature at the EAR can be seen up to 62 keV and is therefore consistent with the above estimations.

Whistler waves upstream of the shock, predominantly propagate away from the shock along the magnetic field lines (Lalti, Khotyaintsev, Graham, et al., 2022). In the wave frame, electrons are pitch-angle scattered while their energy is conserved. This implies that a magnetic bottle-trapped electron, impinging on the shock, will experience the magnetic mirror moving at a greater speed (shock speed plus whistler phase speed) than in the adiabatic case (only the shock speed). This adds to an already effective acceleration process and makes it even more effective, and can help explain the large increase in flux observed at the EAR.

An alternative to consider is whether the EAR is due to reflections between the shock and the upstream turbulence observed from 11:51:50 to 11:52:10 in Figure 1a. However, the near-perfect symmetry of the bi-directional signal (EAR) suggests both mirrors reflect particles with similar efficiency, as would be the case for the scenario described in this letter (shock as both mirrors). If one of the mirrors was the upstream turbulent region, the bi-directional signature at the EAR should be observed all the way up to the encounter with the turbulent region but, is not. More importantly, one would expect a clear asymmetry between the two field-aligned populations. The wave amplitudes

turbulence interacting with a shock can cause strong perturbations in its shape and have a great impact on particle acceleration (Trotta et al., 2022). Therefore, it is not impossible but rather rare for the suggested configuration to occur at Earth's bow shock. Which is consistent with the atypical nature of the event.

The small separation of MMS and the dynamic and complex nature of the bow shock further complicate the geometric analysis of the field line/shock configuration. Future simulations can be used to compare the data presented in this paper and provide powerful insight into this theory.

The data used in this paper were obtained from the Fast Plasma Investigation (Pollock et al., 2016), Flux Gate Magnetometer (Russell et al., 2016), Search Coil Magnetometer (Le Contel et al., 2016) and Fly's Eye Energetic Particle Spectrometer (FEEPS) (Blake et al., 2016). The OMNI data were obtained from the OMNIWeb interface at <https://omniweb.gsfc.nasa.gov> (King & Papitashvili, 2005).

Data Availability Statement

All data can be obtained from the MMS Science Data Center (<https://asp.colorado.edu/mms/sdc/public/about/browse-wrapper/>). Data analysis was performed using the IRFU-Matlab analysis package <https://github.com/irfu/irfu-matlab/>.

References

- Amano, T., & Hoshino, M. (2022). Theory of electron injection at oblique shock of finite thickness. *The Astrophysical Journal*, 927(1), 132. <https://doi.org/10.3847/1538-4357/ac4f49>
- Amano, T., Katou, T., Kitamura, N., Oka, M., Matsumoto, Y., Hoshino, M., et al. (2020). Observational evidence for stochastic shock drift acceleration of electrons at the Earth's bow shock. *Physical Review Letters*, 124(6), 065101. <https://doi.org/10.1103/PhysRevLett.124.065101>
- Balikhin, M. A., Krasnosel'skikh, V. V., & Woolliscroft, L. J. C. (1989). Reflection of electrons from the front of a strong quasiperpendicular shock and the generation of plasma waves. *Advances in Space Research*, 9(4), 203–206. [https://doi.org/10.1016/0273-1177\(89\)90115-4](https://doi.org/10.1016/0273-1177(89)90115-4)
- Balogh, A., & Treumann, R. A. (2013a). Basic equations and models. In A. Balogh & R. A. Treumann (Eds.), *Physics of collisionless shocks: Space plasma shock waves* (pp. 45–123). Springer New York. https://doi.org/10.1007/978-1-4614-6099-2_3
- Balogh, A., & Treumann, R. A. (2013b). Particle acceleration. In A. Balogh & R. A. Treumann (Eds.), *Physics of collisionless shocks: Space plasma shock waves* (pp. 333–398). Springer New York. https://doi.org/10.1007/978-1-4614-6099-2_7
- Balogh, A., & Treumann, R. A. (2013c). Quasi-parallel supercritical shocks. In A. Balogh & R. A. Treumann (Eds.), *Physics of collisionless shocks: Space plasma shock waves* (pp. 221–331). Springer New York. https://doi.org/10.1007/978-1-4614-6099-2_6
- Bamba, A., Yamazaki, R., & Hiraga, J. S. (2005). Chandra observations of galactic supernova remnant Vela Jr.: A new sample of thin filaments emitting synchrotron X-rays. *The Astrophysical Journal*, 632(1), 294–301. <https://doi.org/10.1086/432711>
- Bame, S. J., Asbridge, J. R., Feldman, W. C., Gosling, J. T., & Zwickl, R. D. (1981). Bi-directional streaming of solar wind electrons > 80 eV: ISEE evidence for a closed-field structure within the driver gas of an interplanetary shock. *Geophysical Research Letters*, 8(2), 173–176. <https://doi.org/10.1029/GL008i002p00173>
- Blake, J. B., Mauk, B. H., Baker, D. N., Carranza, P., Clemmons, J. H., Craft, J., et al. (2016). The fly's eye energetic particle spectrometer (FEEPS) sensors for the magnetospheric multiscale (MMS) mission. *Space Science Reviews*, 199(1), 309–329. <https://doi.org/10.1007/s11214-015-0163-x>
- Blandford, R., & Eichler, D. (1987). Particle acceleration at astrophysical shocks: A theory of cosmic ray origin. *Physics Reports*, 154(1), 1–75. [https://doi.org/10.1016/0370-1573\(87\)90134-7](https://doi.org/10.1016/0370-1573(87)90134-7)
- Bohdan, A., Pohl, M., Niemiec, J., Vafin, S., Matsumoto, Y., Amano, T., & Hoshino, M. (2020). Kinetic simulations of nonrelativistic perpendicular shocks of young supernova remnants. III. Magnetic reconnection. *The Astrophysical Journal*, 893(1), 6. <https://doi.org/10.3847/1538-4357/ab7cd6>
- Burgess, D. (2006). Simulations of electron acceleration at collisionless shocks: The effects of surface fluctuations. *The Astrophysical Journal*, 653(1), 316–324. <https://doi.org/10.1086/508805>
- Burgess, D., Lucek, E. A., Scholer, M., Bale, S. D., Balikhin, M. A., Balogh, A., et al. (2005). Quasi-parallel shock structure and processes. *Space Science Reviews*, 118(1), 205–222. <https://doi.org/10.1007/s11214-005-3832-3>
- Crooker, N., Gosling, J., Bothmer, V., Forsyth, R., Gazis, P., Hewish, A., et al. (1999). CIR morphology, turbulence, discontinuities, and energetic particles. *Space Science Reviews*, 89(1), 179–220. <https://doi.org/10.1023/A:1005253526438>
- Decker, R. B. (1993). The role of magnetic loops in particle acceleration at nearly perpendicular shocks. *Journal of Geophysical Research*, 98(A1), 33–46. <https://doi.org/10.1029/92JA01841>
- Dresing, N., Kouloumvakos, A., Vainio, R., & Rouillard, A. (2022). On the role of coronal shocks for accelerating solar energetic electrons. *The Astrophysical Journal Letters*, 925(2), L21. <https://doi.org/10.3847/2041-8213/ac4ca7>
- Dresing, N., Theesen, S., Klassen, A., & Heber, B. (2016). Efficiency of particle acceleration at interplanetary shocks: Statistical study of STEREO observations. *Astronomy & Astrophysics*, 588, A17. <https://doi.org/10.1051/0004-6361/201527853>
- Fairfield, D. H. (1971). Average and unusual locations of the Earth's magnetopause and bow shock. *Journal of Geophysical Research*, 76(28), 6700–6716. <https://doi.org/10.1029/JA076i028p06700>
- Fitzenreiter, R. J. (1995). The electron foreshock. *Advances in Space Research*, 15(8), 9–27. [https://doi.org/10.1016/0273-1177\(94\)00081-B](https://doi.org/10.1016/0273-1177(94)00081-B)
- Formisano, V. (1979). Orientation and shape of the Earth's bow shock in three dimensions. *Planetary and Space Science*, 27(9), 1151–1161. [https://doi.org/10.1016/0032-0633\(79\)90135-1](https://doi.org/10.1016/0032-0633(79)90135-1)
- Giacalone, J. (2005). The efficient acceleration of thermal protons by perpendicular shocks. *The Astrophysical Journal*, 628(1), L37–L40. <https://doi.org/10.1086/432510>
- Guo, F., & Giacalone, A. J. (2015). The acceleration of electrons at collisionless shocks moving through a turbulent magnetic field. *The Astrophysical Journal*, 802(2), 97. <https://doi.org/10.1088/0004-637X/802/2/97>

Acknowledgments

This work is supported by the Swedish Research Council Grant 2018-05514. The authors thank the entire MMS team for the design and continuing operation of the mission.

- Gurnett, D. A., & Bhattacharjee, A. (2005). *Introduction to plasma physics: With space and laboratory applications* (1st ed.). Cambridge University Press.
- Hoshino, M., & Shimada, N. (2002). Nonthermal electrons at high Mach number shocks: Electron shock surfing acceleration. *The Astrophysical Journal*, 572(2), 880–887. <https://doi.org/10.1086/340454>
- Johlander, A., Battarbee, M., Vaivads, A., Turc, L., Pfau-Kempf, Y., Ganse, U., et al. (2021). Ion acceleration efficiency at the Earth's bow shock: Observations and simulation results. *The Astrophysical Journal*, 914(2), 82. <https://doi.org/10.3847/1538-4357/abfabc>
- Johlander, A., Schwartz, S. J., Vaivads, A., Khotyaintsev, Y. V., Gingell, I., Peng, I. B., et al. (2016). Rippled quasiperpendicular shock observed by the magnetospheric multiscale spacecraft. *Physical Review Letters*, 117(16), 165101. <https://doi.org/10.1103/PhysRevLett.117.165101>
- Johlander, A., Vaivads, A., Khotyaintsev, Y. V., Gingell, I., Schwartz, S. J., Giles, B. L., et al. (2018). Shock ripples observed by the MMS spacecraft: Ion reflection and dispersive properties. *Plasma Physics and Controlled Fusion*, 60(12), 125006. <https://doi.org/10.1088/1361-6587/aae920>
- Kajdič, P., Pfau-Kempf, Y., Turc, L., Dimmock, A. P., Palmroth, M., Takahashi, K., et al. (2021). ULF wave transmission across collisionless shocks: 2.5D local hybrid simulations. *Journal of Geophysical Research: Space Physics*, 126(11), e2021JA029283. <https://doi.org/10.1029/2021JA029283>
- Kajdič, P., Preisser, L., Blanco-Cano, X., Burgess, D., & Trotta, D. (2019). First observations of irregular surface of interplanetary shocks at ion scales by cluster. *The Astrophysical Journal*, 874(2), L13. <https://doi.org/10.3847/2041-8213/ab0e84>
- Katou, T., & Amano, T. (2019). Theory of stochastic shock drift acceleration for electrons in the shock transition region. *The Astrophysical Journal*, 874(2), 119. <https://doi.org/10.3847/1538-4357/ab0d8a>
- King, J. H., & Papitashvili, N. E. (2005). Solar wind spatial scales in and comparisons of hourly Wind and ACE plasma and magnetic field data. *Journal of Geophysical Research*, 110(A2), A02104. <https://doi.org/10.1029/2004ja010649>
- Koyama, K., Petre, R., Gotthelf, E. V., Hwang, U., Matsuura, M., Ozaki, M., & Holt, S. S. (1995). Evidence for shock acceleration of high-energy electrons in the supernova remnant SN1006. *Nature*, 378(6554), 255–258. <https://doi.org/10.1038/378255a0>
- Krauss-Varban, D., Burgess, D., & Wu, C. S. (1989). Electron acceleration at nearly perpendicular collisionless shocks. I: One-dimensional simulations without electron scale fluctuations. (Vol. 94, pp. 15.089–15.098). <https://doi.org/10.1029/ja094ia11p15089>
- Lalti, A., Khotyaintsev, Y. V., Dimmock, A. P., Johlander, A., Graham, D. B., & Olshevsky, V. (2022). A database of MMS bow shock crossings compiled using machine learning. *Journal of Geophysical Research: Space Physics*, 127(8), e2022JA030454. <https://doi.org/10.1029/2022JA030454>
- Lalti, A., Khotyaintsev, Y. V., Graham, D. B., Vaivads, A., Steinvall, K., & Russell, C. T. (2022). Whistler waves in the foot of Quasi-perpendicular supercritical shocks. *Journal of Geophysical Research: Space Physics*, 127(5), e2021JA029969. <https://doi.org/10.1029/2021JA029969>
- Le Contel, O., Leroy, P., Roux, A., Coillot, C., Alison, D., Bouabdellah, A., et al. (2016). The search-coil magnetometer for MMS. *Space Science Reviews*, 199(1), 257–282. <https://doi.org/10.1007/s11214-014-0096-9>
- Lembège, B., & Savoini, P. (2002). Formation of reflected electron bursts by the nonstationarity and nonuniformity of a collisionless shock front. *Journal of Geophysical Research*, 107(A3), SMPX-1–SMPX-18. <https://doi.org/10.1029/2001JA900128>
- Leroy, M. M., & Mangeney, A. (1984). A theory of energization of solar wind electrons by the Earth's bow shock. *Annales Geophysicae*, 2, 449–456.
- Madanian, H., Desai, M. I., Schwartz, S. J., Wilson, L. B., Fuselier, S. A., Burch, J. L., et al. (2021). The dynamics of a high Mach number Quasi-perpendicular shock: MMS observations. *The Astrophysical Journal*, 908(1), 40. <https://doi.org/10.3847/1538-4357/abc888>
- Matsumoto, Y., Amano, T., Kato, T. N., & Hoshino, M. (2017). Electron surfing and drift accelerations in a Weibel-dominated high-Mach-number shock. *Physical Review Letters*, 119(10), 105101. <https://doi.org/10.1103/PhysRevLett.119.105101>
- Meziane, K. (2005). A review of field-aligned beams observed upstream of the bow shock. In *AIP conference proceedings*. In Palm springs (Vol. 781, pp. 116–122). AIP. <https://doi.org/10.1063/1.2032683>
- Palmer, I. D., Allum, F. R., & Singer, S. (1978). Bidirectional anisotropies in solar cosmic ray events: Evidence for magnetic bottles. *Journal of Geophysical Research*, 83(A1), 75–90. <https://doi.org/10.1029/JA083iA01p00075>
- Paschmann, G., & Daly, P. W. (2000). *Analysis methods for multi-spacecraft data* (p. 536).
- Peredó, M., Slavin, J. A., Mazur, E., & Curtis, S. A. (1995). Three-dimensional position and shape of the bow shock and their variation with Alfvénic, sonic and magnetosonic Mach numbers and interplanetary magnetic field orientation. *Journal of Geophysical Research*, 100(A5), 7907–7916. <https://doi.org/10.1029/94JA02545>
- Perri, S., & Zimbaro, G. (2012). Magnetic variances and pitch-angle scattering times upstream of interplanetary shocks. *The Astrophysical Journal*, 754(1), 8. <https://doi.org/10.1088/0004-637X/754/1/8>
- Pollock, C., Moore, T., Jacques, A., Burch, J., Gliese, U., Saito, Y., et al. (2016). Fast plasma investigation for magnetospheric multiscale. *Space Science Reviews*, 199(1), 331–406. <https://doi.org/10.1007/s11214-016-0245-4>
- Pulupa, M. P., Bale, S. D., & Salem, C. (2011). An asymmetry of the electron foreshock due to the strahl. *Geophysical Research Letters*, 38(14), L14105. <https://doi.org/10.1029/2011GL048029>
- Retinò, A., Khotyaintsev, Y., Le Contel, O., Marcucci, M. F., Plaschke, F., Vaivads, A., et al. (2021). Particle energization in space plasmas: Towards a multi-point, multi-scale plasma observatory. *Experimental Astronomy*. <https://doi.org/10.1007/s10686-021-09797-7>
- Russell, C. T., Anderson, B. J., Baumjohann, W., Bromund, K. R., Dearborn, D., Fischer, D., et al. (2016). The magnetospheric multiscale magnetometers. *Space Science Reviews*, 199(1), 189–256. <https://doi.org/10.1007/s11214-014-0057-3>
- Slavin, J. A., & Holzer, R. E. (1981). Solar wind flow about the terrestrial planets I. Modeling bow shock position and shape. *Journal of Geophysical Research*, 86(A13), 11401–11418. <https://doi.org/10.1029/JA086iA13p11401>
- Stasiewicz, K., & Klos, Z. (2022). On the formation of quasi-parallel shocks, magnetic and electric field turbulence, and the ion energisation mechanism. *Monthly Notices of the Royal Astronomical Society*, 513(4), 5892–5899. <https://doi.org/10.1093/mnras/stac1193>
- Trotta, D., & Burgess, D. (2019). Electron acceleration at quasi-perpendicular shocks in sub- and supercritical regimes: 2D and 3D simulations. *Monthly Notices of the Royal Astronomical Society*, 482(1), 1154–1162. <https://doi.org/10.1093/mnras/sty2756>
- Trotta, D., Valentini, F., Burgess, D., & Servidio, S. (2021). Phase space transport in the interaction between shocks and plasma turbulence. *Proceedings of the National Academy of Sciences of the United States of America*, 118(21), e2026764118. <https://doi.org/10.1073/pnas.2026764118>
- Trotta, D., Vuorinen, L., Hietala, H., Horbury, T., Dresing, N., Gieseler, J., et al. (2022). Single-spacecraft techniques for shock parameters estimation: A systematic approach. *Frontiers in Astronomy and Space Sciences*, 9. <https://doi.org/10.3389/fspas.2022.1005672>
- Turner, D. L., Fennell, J. F., Blake, J. B., Clemmons, J. H., Mauk, B. H., Cohen, I. J., et al. (2016). Energy limits of electron acceleration in the plasma sheet during substorms: A case study with the Magnetospheric Multiscale (MMS) mission. *Geophysical Research Letters*, 43(15), 7785–7794. <https://doi.org/10.1002/2016GL069691>

- Vandas, M. (2001). Shock drift acceleration of electrons: A parametric study. *Journal of Geophysical Research*, *106*(A2), 1859–1871. <https://doi.org/10.1029/2000JA900128>
- Vasko, I. Y., Mozer, F. S., Krasnoselskikh, V. V., Artemyev, A. V., Agapitov, O. V., Bale, S. D., et al. (2018). Solitary waves across supercritical Quasi-perpendicular shocks. *Geophysical Research Letters*, *45*(12), 5809–5817. <https://doi.org/10.1029/2018GL077835>
- Wilson, L. B., Sibeck, D. G., Turner, D. L., Osmane, A., Caprioli, D., & Angelopoulos, V. (2016). Relativistic electrons produced by foreshock disturbances observed upstream of Earth's bow shock. *Physical Review Letters*, *117*(21), 215101. <https://doi.org/10.1103/PhysRevLett.117.215101>
- Wu, C. S. (1984). A fast Fermi process: Energetic electrons accelerated by a nearly perpendicular bow shock. *Journal of Geophysical Research*, *89*(A10), 8857–8862. <https://doi.org/10.1029/JA089iA10p08857>